Interpretation of Refraction and Reflection Stack

Data Over the Brevard Fault Zone in South Carolina

by

Kenneth J. Laughlin

Thesis submitted to the Faculty of the

Virginia Polytechnic Institute and State University

in partial fulfillment of the requirements for the degree of

Master of Science

in

Geophysics

APPROVED:

Cahit Çoruh, Chairman

John K. Costain

Edwin S. Robinson

January 27, 1988

Blacksburg, Virginia

Interpretation of Refraction and Reflection Stack Data Over the Brevard Fault Zone in South Carolina

by

Kenneth J. Laughlin

Cahit Çoruh, Chairman

Geophysics

(ABSTRACT)

Near surface structures across the Brevard fault zone are studied using the refraction and reflection arrivals recovered from the Appalachian Ultradeep Core Hole (ADCOH) regional seismic Line 1. In using refracted arrivals, a new processing approach is introduced that translates refracted first arrivals from multifold seismic data into a refraction stack of two-way delay time sections. Reprocessing of reflected arrivals has improved shallow reflectors and allowed better imaging of the Brevard fault zone. Following processing of refraction and reflection arrivals independently, both data sets are combined into a composite stack section. The composite stack section displays one bright refractor interpreted as the boundary between the weathered layer and high velocity crystalline rocks. This refractor is continuous in the Inner Piedmont with occasional vertical offsets. The continuity of the refractor diminishes across the Brevard fault zone. In the eastern Blue Ridge, the refractor is discontinuous with high angle truncations. On the composite stack section, the Brevard fault zone can be traced from the surface to 6 km (2 s) where it appears to splay from the Blue Ridge thrust. Different from previous interpretations, the Brevard fault zone is imaged as having both an upper and a lower boundary surface as well as a group of reflectors within the zone. This reflection package initially thickens to 2 km at 3 km depth, then thins as it reaches the Blue Ridge master decollement. The Blue Ridge thrust is as shallow as 1.5 km (0.5 s) at the northwest end of the Line 1. A deeper decollement is interpreted below the Blue Ridge thrust. The depth of this deeper thrust is 3 km (1 s) at the northwest end of the line, and also joins to the Blue Ridge thrust at 6 km depth making the structures below the Brevard fault zone more complex than previously published.

Acknowledgements

The seismic reflection data were acquired by Western Geophysical Company for the Appalachian Ultradeep Core Hole (ADCOH) site study project. Funding was provided by NSF Grant EAR-8417894 in support of work by R.D. Hatcher at The University of South Carolina (presently at The University of Tennessee, Knoxville) and J.K. Costain, C. Çoruh, and L. Glover, III, all at Virginia Polytechnic Institute and State University. Seismic data processing was conducted using Cogniseis's DISCO seismic processing software on the VAX 11/780 computer at the Regional Geophysics Laboratory, Virginia Polytechnic Institute and State University, Blacksburg, Virginia.

Financial support for this graduate adventure was provided by ARCO and the Department of Geological Sciences. Academic support was provided by my fellow graduate students especially all the people in 1070. Many thanks go to for all her time spent with me on all my projects, and to for keeping most everything on this side of campus in operating order.

I need to express appreciation to Cahit Çoruh, my committee chairman, for innumerable hours spent developing this project and keeping it moving. Special thanks to my other committee

members, John Costain and Edwin Robinson. Both Dr. Costain and Dr. Robinson contributed ideas valuable to the development and interpretation of this project. In addition, they were both actively involved in by geophysics coursework as well as the final form of this thesis. I would also like to thank Drs G.A. Bollinger and J.A. Snoke for their input while I was here. Also, thanks go to and , from The University of Tennessee, Knoxville, for providing input about the surface geology in the study area.

Finally, I would like to give thanks to all of my friends for the times spent and to my family .... , , , , , , , and most of all my mother . I have learned lessons in success from all of them and for that I dedicate this thesis.

Table of Contents

Introduction 1

Available Seismic Data 8
COCORP data 10
Seisdata reflection data 10

Seismic Data Processing 13
Refracted Arrivals 13
Reflected Arrivals 18
Combined Refraction and Reflection Stacks 18

Discussion and Interpretation 24
Ability of Refraction Stacks to Image the Subsurface 24
Correlation of available data sets 26
Interpretations 28

Conclusions 37

Bibliography 39

Appendix 41

Vita 42

List of Illustrations

Figure 1. Location map for ADCOH, COCORP, and Seisdata seismic lines 5
Figure 2. ADCOH Line1 and HI-RES 8 seismic profiles 6
Figure 3. COCORP and Seisdata seismic profiles 7
Figure 4. ADCOH Line 1 noise test 12
Figure 5. Concept of the refraction stack processing 20
Figure 6. Refraction stack processing 21
Figure 7. Constant velocity refraction stack (CVRS) panels 22
Figure 8. Residual statics improvements in refraction stack sections 22
Figure 9. Portion of reprocessed ADCOH regional 23
Figure 10. Refraction stack sections with surface elevation plots 31
Figure 11. Fault signature in shot gathers 32
Figure 12. Travel time-offset (t-x) curve of noise test. 33
Figure 13. Portion of the composite stack section 34
Figure 14. Portion of the composite stack section after migration 35
Figure 15. Final automatic line drawing from composite stack section 36

Introduction

The purpose of this study is to examine further near surface structures across the Brevard fault zone (Figure 1) in South Carolina by using refracted and reflected arrivals from the Appalachian Ultradeep Core Hole (ADCOH) project multi-fold seismic data.

The primary goal of the ADCOH project is to examine the basic tectonic processes and crustal structure of a composite crystalline thrust sheet formed by continental collision. Because composite crystalline thrust sheets are among the largest structures in orogenic belts, they are important to the overall processes involved with mountain building and the evolution of continental crust (Hatcher and others, in press). The subsurface image of the BFZ has been one of the important targets of the site selection of the ADCOH project. The 10-12 km ultradeep core hole will sample the Brevard fault zone (BFZ) permitting comparative structural and thermochemical/isotopic studies of the formation of ductile and brittle fault zone with multiple displacements.

The general study area (Figure 1), located in Oconee County South Carolina near the town of Westminster, encompasses three major tectonic provinces over which a considerable amount of geological-geophysical investigations have been completed. From southeast to northwest in Figure 1 these provinces are: (1) the crystalline Inner Piedmont allochthon and Chauga Belt; (2)

the Brevard fault zone (BFZ); and (3) the crystalline Blue Ridge allochthon (BRA). Across these three tectonic provinces a distinct assemblage of rock types have been studied (Hatcher, 1971). Within the Brevard fault zone, rocks are pervasively sheared mylonites, ultramylonites, blastomylonites, and phyllonites (Hatcher, 1971). The Inner Piedmont rocks in the study area consist largely of granitic gneiss, amphibolite, and biotite gneiss. Studies of the Chauga Belt rocks indicate that they are of lower grade than the high grade terranes of the eastern Blue Ridge and Inner Piedmont. These are composed of augen gneiss and lineated granitic gneiss. The eastern Blue Ridge geologic province is predominately granitic gneiss, biotite schist and biotite gneiss, hornblende gneiss, and upper amphibolite facies of metavolcanic and metasedimentary rocks (Hadley and Nelson, 1971).

Both the Blue Ridge allochthon as well as the Inner Piedmont and Chauga Belt are proposed to have been displaced northwest along the Blue Ridge master decollement for tens to hundreds of kilometers (Bryant and Reed, 1970). Hatcher (1971) further proposed that the BFZ formed from failure on the northwest limb of the Low Rank Belt Synclinorium due to motion along the Blue Ridge thrust. The fault initiation, which separated the Inner Piedmont allochthon and Chauga Belt from the Blue Ridge allochthon, occurred within incompetent rocks in the northwest limb (Hatcher, 1971). According to Cook and others (1979), the displacement along the Blue Ridge master decollement could be as great as 260 kilometers. Hatcher and others (1987a) indicate that this displacement is significantly greater.

The Brevard fault zone is mapped as a narrow linear belt of intense shearing and faulting from the Alabama Piedmont to near the North Carolina-Virginia border. Due to motion on the fault, a variety of different lithologies can be found within a small traverse across the BFZ. Because of this, the Brevard fault zone has long been considered a significant Appalachian orogenic boundary, in addition to a major crustal failure (Jonas, 1932; King, 1955; Reed and Bryant, 1964; Bryant and Reed, 1970; Hatcher 1971; Hatcher and others 1987a; and Hatcher and others 1987b). The Brevard as a thrust was first presented by Jonas (1932).

Imaging of the Brevard fault zone using seismic reflection data was reported with different emphasis in the literature. Successful imaging of reflections from the BFZ was first published by Clark and others in 1978 closely followed by Cook and others (1979) with results from combined COCORP reflection profiles. Seisdata seismic profiles with line drawings and interpretations of the Brevard zone were published by Behrendt in 1986. Better images of the BFZ were recovered from the collection of ADCOH seismic data (Çoruh and others, 1987; Chowdhury and Phinney, 1987).

The seismic characteristics of the Brevard fault zone as determined by these studies have been imaged differently in each data set. Using velocity spectra, Clark and others (1978) recovered reflections from the top and bottom of the BFZ, near Rosman N.C., giving the BFZ a thickness of 0.9 km with a velocity of 5.9 km/sec. On the other hand, interpretations of COCORP data in Georgia by Cook and others (1979) show the BFZ as a single discontinuous group of reflectors rooted in the Blue Ridge master decollement (BRMD). Behrendt's (1986) interpretation of the BFZ from Seisdata lines is as a series of southeastward dipping reflections. ADCOH regional Line 1 (Çoruh and others, 1987) define the BFZ as a zone of east dipping reflectors between highly reflective Inner Piedmont and poorly reflective Blue Ridge rocks. The high resolution ADCOH seismic profile (Chowdhury and Phinney, 1987) again image the BFZ as a zone, with a maximum vertical thickness of 0.4 s (1.2 km), having distinct top and bottom reflectors.

Despite all these studies, the first 0.6 s (1.8 km) part of the BFZ was in question. While imaged well at depth, few continuous reflections were observed in the first 0.6 s on ADCOH regional Line 1 (Figure 2a) and the first full second is not published on ADCOH high resolution Line 8 (Figure 2b). On both COCORP line GA1 (Figure 3a) and Seisdata Lines 6 and 8 (Figure 3b) only deep reflections were observed.

To correlate the imaged part of the BFZ with surface geology, shallow seismic data were considered to be essential. In this paper, an attempt is made to image the geometry of the subsurface structure of the BFZ by using both refracted and reflected arrivals from the ADCOH regional Line

1 data set. The refraction and reflection arrivals are processed, evaluated, and interpreted. The results are three refraction stack sections of refracted first arrivals, reduced to delay time for the entire ADCOH regional Line 1, reprocessed reflection stack sections (unmigrated and migrated) from CMP 710 to 1680 to a depth of 4 seconds, and a combined refraction and migrated reflection stack section. The different refraction stack sections with different offset ranges and fold illustrate different degree of smoothing effects. Composite stacks as a combination of specific refraction and reflection stack sections are used for final interpretation. This final interpretation also incorporates results from surface geology, shallow core hole data, and a noise test.

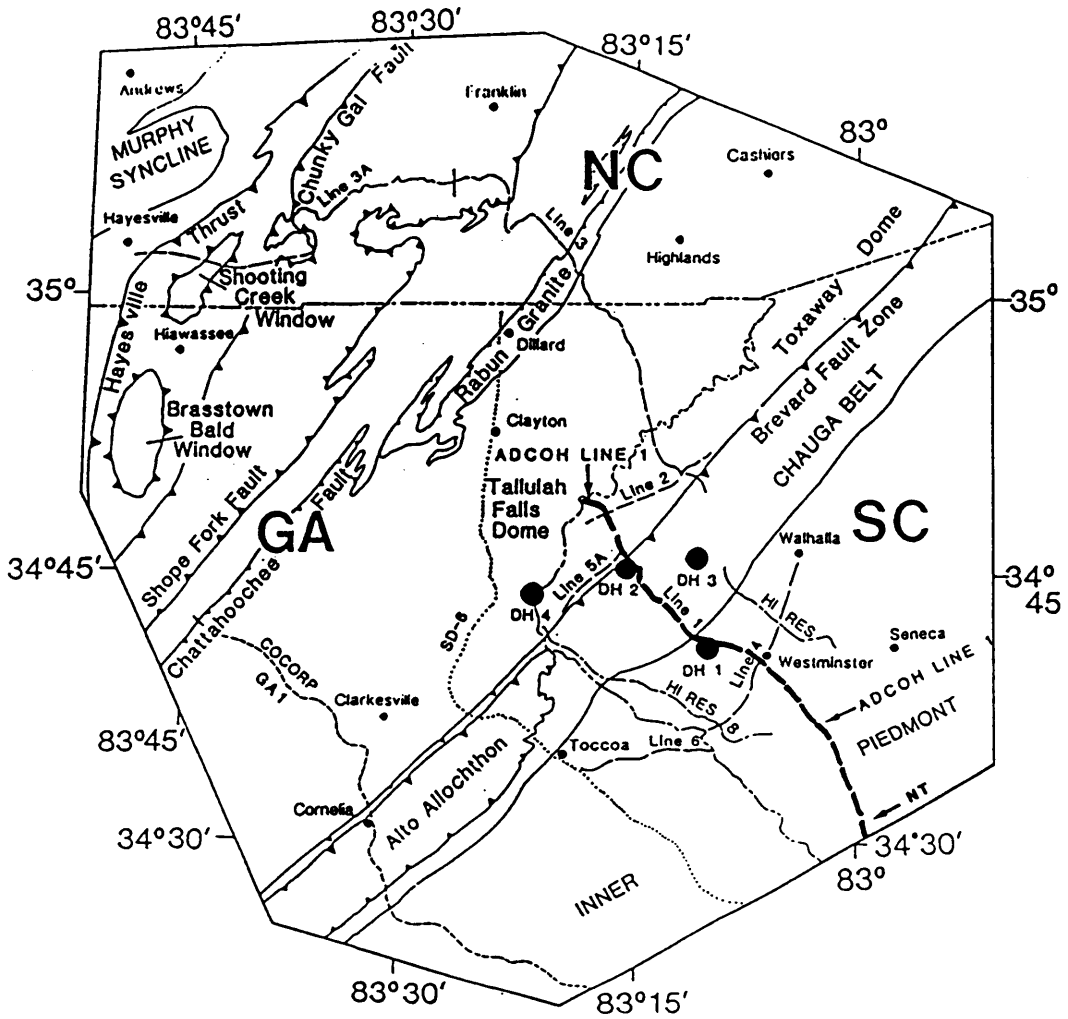

Figure 1. Location map for ADCOH, COCORP, and Seisdata seismic lines: (from Hatcher and others, 1987). ADCOH regional Line 1 is highlighted with thick dashed lines and labelled as Line 1; ADCOH high resolution Line 8 is HI-RES 8; the COCORP seismic line is COCORP GA1; and Seisdata Lines are displayed as SD-6 and SD-8. NT indicates the location of the noise test on Line 1.

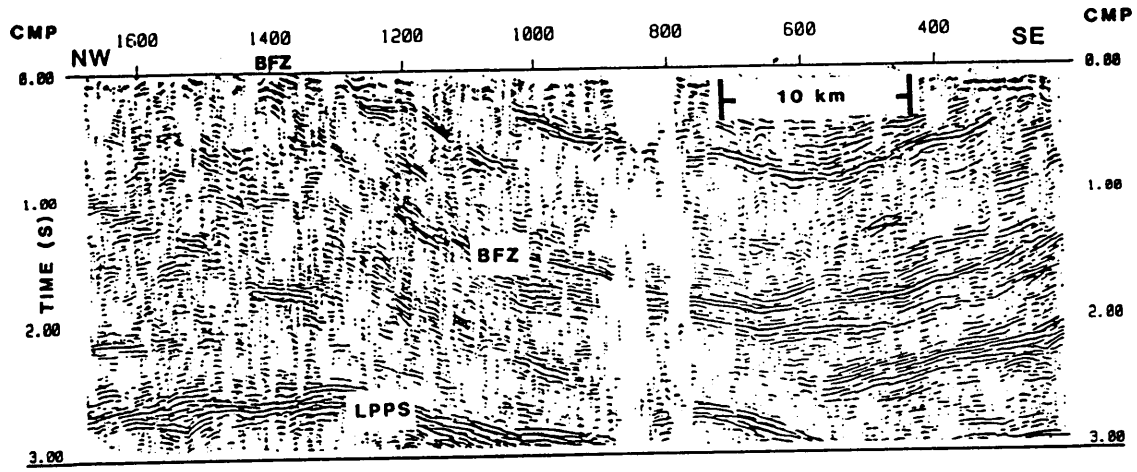

(a)

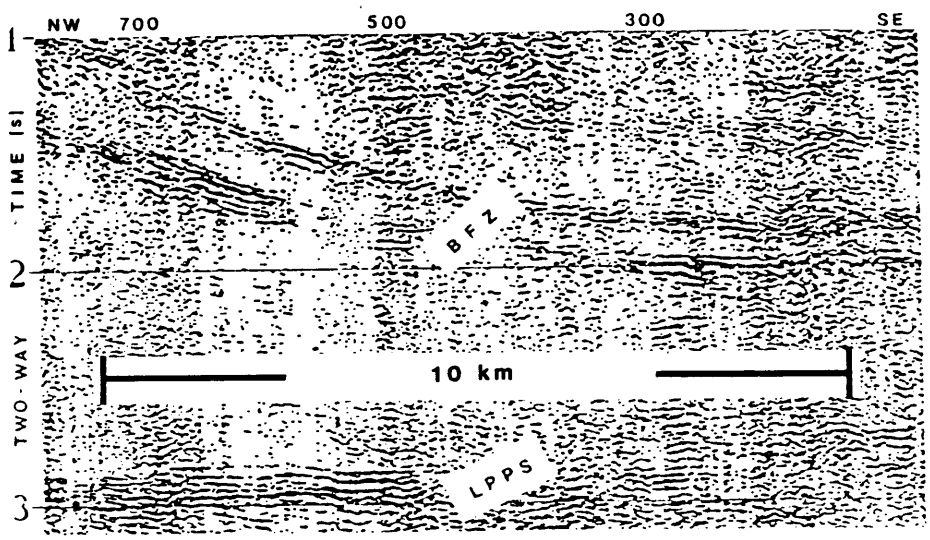

(b)

Figure 2. **ADCOH Line1 and HI-RES 8 seismic profiles:** (a) ADCOH regional Line 1 automatic line drawing (from Çoruh and others, 1987). (b) ADCOH HI-RES 8 section (from Chowdhury and Phinney, 1987) begins at 1 s depth at which the Brevard fault zone is approximately 0.4 s thick. The BFZ and lower Paleozoic platform sediments (LPPS) are well imaged in both sections below 1 s.

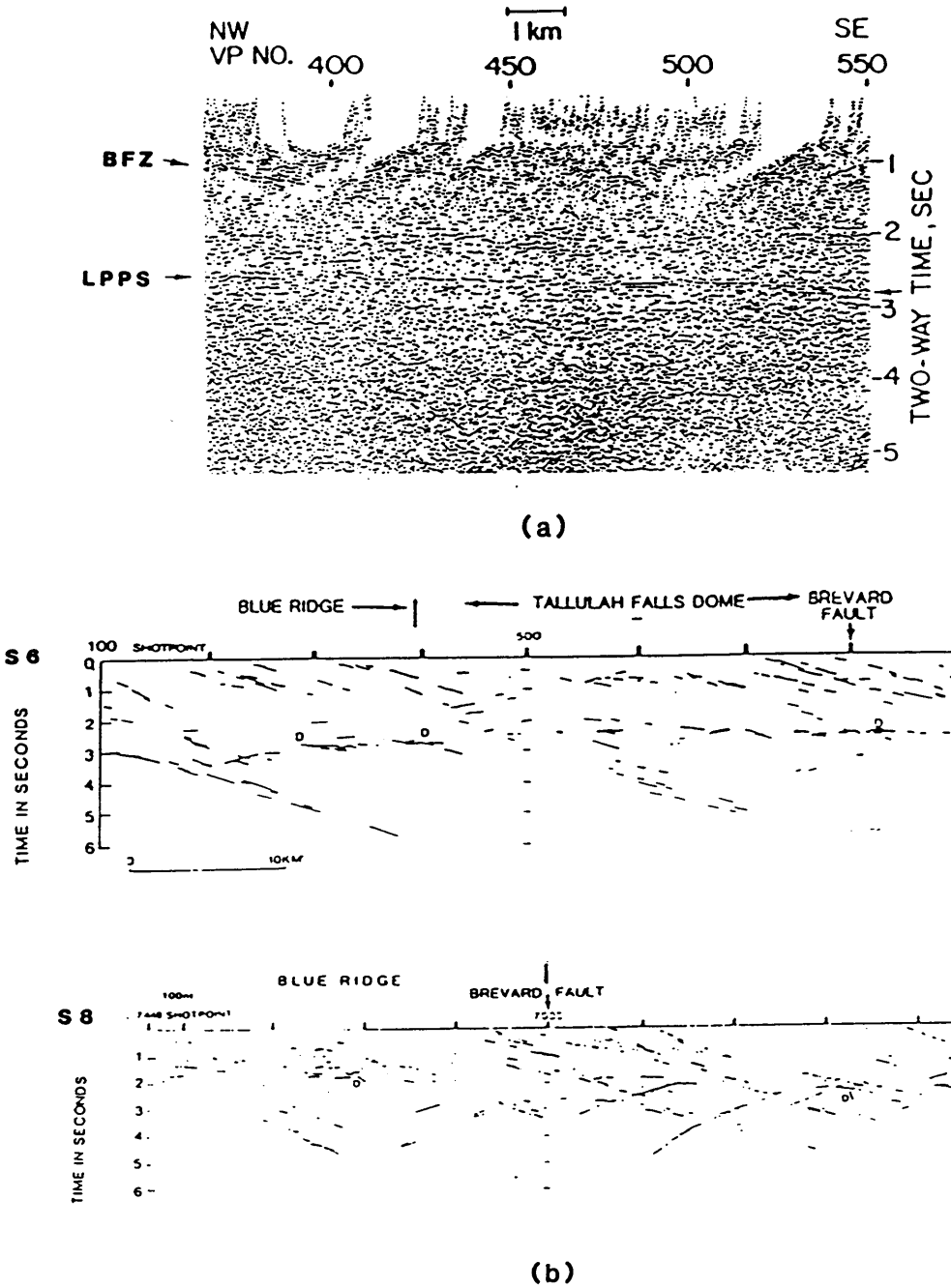

Figure 3. COCORP and Seisdata seismic profiles: (a) COCORP Line GA1 (from Cook and others, 1979) in vicinity of the Brevard fault zone reflections. Top arrow indicates reflections from the Brevard fault zone. Lower arrow denotes lower Paleozoic platform sediments. (b) Line drawing interpretations of SD-6 and SD-8 (from Behrendt, 1986). Brevard fault zone reflections are indicated as eastward dipping reflections packages. All three of these data sets image few shallow reflections or reflections from the Brevard fault zone.

Available Seismic Data

A short description of the data sets acquired near the study area with information relative to the BFZ is given below. The ADCOH regional data set contains 180 km of vibroseis profiles that were acquired by Western Geophysical Company in Georgia and South Carolina (Figure 1) for the ADCOH project.

ADCOH regional Line 1 data acquisition was conducted with 120-channel recording system and five vibrators using 24 s up-sweeps with 14-56 Hz. The recording time was 32 s to give 8 s of full-correlation time. Spread configuration was a symmetrical split-spread with near and far offsets of 200 and 4150 m. Receiver groups consisted of twenty-four 10 Hz digital grade geophones covering 0.134 km in length and spaced at 0.067 km group intervals. Shot intervals were also 0.067 km giving a maximum subsurface coverage of 60 fold. Because of higher signal-to-noise ratio of the ADCOH regional lines and their availability, the ADCOH regional Line 1 is used in this study.

Prior to collecting Line 1, a noise test was conducted at the beginning of the line ("NT" in Figure 1) within Inner Piedmont rocks. The noise test geometry was straight line with bunched receiver groups spaced at 0.003 km intervals. 5.4 km of coverage were obtained in 16 records to give 0.07 km and 5.4 km near and far offsets. The source was a single vibrator with 8-56 Hz up-

sweeps. The resulting shot ordered, as continuous one-fold, data are shown in Figure 4. This data set is used as a key to interpret the refracted arrivals of the ADCOH regional Line 1.

ADCOH Line 1 was originally processed at the Regional Geophysics Laboratory at Virginia Tech and published in the forms of conventional sections to a depth of 8 s (Costain and others, 1986) and automatic line drawings to a depth of 14 s (Çoruh and others 1987). The imaging quality of the data is among one of the best over crystalline terrane and possible interpretations and their implications are also discussed by Hatcher and others (1987b). Interpreted from Line 1 are the Blue Ridge thrust (BRT) and the Brevard fault zone which appears to splay from the BRT at 6 km depth. The BFZ is interpreted as a group of eastward dipping reflectors, from a depth of approximately 0.6 s (1.8 km) to 2 s (6 km) respectively, bounded by the highly reflective Inner Piedmont and the relatively transparent Blue Ridge (Çoruh and others, 1987). Most importantly, the BFZ was imaged to separate the highly reflective Inner Piedmont rocks from the poorly reflective Blue Ridge rocks. The BFZ splays into the BRT at a depth of 1.8 s (5.4 km). Additionally, subhorizontal reflections interpreted as nearly undisturbed lower Paleozoic platform sediments (LPPS) as well as Eocambrian-Cambrian(?) rift basins are well represented in the line drawings at approximate depth 2.6 s (7.8 km).

ADCOH high resolution Line 8 (Figure 1) was acquired using 120 receiver groups at 0.033 km intervals leading to a 4 km spread. The source pickets were 0.033 km apart with 16 intermediate vibrator points with coverage ranging from 30 to 60 fold. A nonlinear sweep of 20-80 Hz was applied for 27 s giving 5 s of full-correlation time (Chowdhury and Phinney, 1987).

The published results of ADCOH high resolution Line 8 display part of the unmigrated preliminary stack section from 1 s to 3 s two-way traveltime (Chowdhury and Phinney, 1987). Clearly imaged in this section are two reflectors from 1 s (3 km) to 2 s (6 km), interpreted as the top and bottom boundary of the Brevard fault zone, separated by a region of seismic transparency of 0.4 s (1.2 km) maximum thickness. These reflected events are furthest apart at 1 s while closest together

at 2 s depth. This geometric configuration of the BFZ indicates a low angle thrust rooted in the BRT at approximately 6 km depth.

COCORP data

COCORP Georgia Line GA1 (Figure 1) was recorded with a 30 s sweep of 8-32 Hz for 15 s of full-correlation data. Cook and others (1979) state that the BFZ does not extend beneath 2 s two-way traveltime (6 km). On GA1, Cook and others (1979) interpret the BFZ to be a single discontinuous package of reflections that dips 16° east and is rooted in the sole thrust BRT (?) above to an apparent offset in the Paleozoic shelf strata beneath beneath the BRT. This relationship supports Hatcher's hypothesis (1971) that thrust ramping along the west flank of the synformal Chauga Belt was initiated by a normal fault in underlying sediments. Additionally, calculations off minimum offset on the Brevard fault zone give 8 km of throw and 30 km heave. The same interpretation for the Brevard fault zone was republished by Brown and others (1986).

Seisdata reflection data

Seisdata seismic reflection data (1350 km of 96 channels) along three profiles in South Carolina and Georgia (Figure 1) were interpreted by Behrendt (1986). The data set has 24 fold maximum coverage and was recorded with a sweep of 48-12 Hz, 24 s long, from four vibrators.

Published line drawing from profiles over the Brevard fault zone display discontinuous dipping reflectors interpreted as the BFZ to a depth of 2 s (Behrendt, 1986). Using the Seisdata reflection seismic data set with the line drawing interpretation of Behrendt (1986) and aeromagnetic profiles, Costain and others (1987) suggested the Brevard fault zone as the "floor" of a large strike-slip duplex that extends approximately 300 km to its root beneath the Atlantic Coastal Plain in North Carolina.

Despite all this published data, the Brevard fault zone at shallower depths was not imaged clearly to give a full correlation with the surface geology. The most shallow image of the BFZ is in the ADCOH regional reflection seismic Line 1 and extends up to 0.6 s depth (Çoruh and others, 1987). Therefore the ADCOH Line 1 data set is reprocessed in this study to obtain an improved image of the Brevard fault zone at shallower depths.

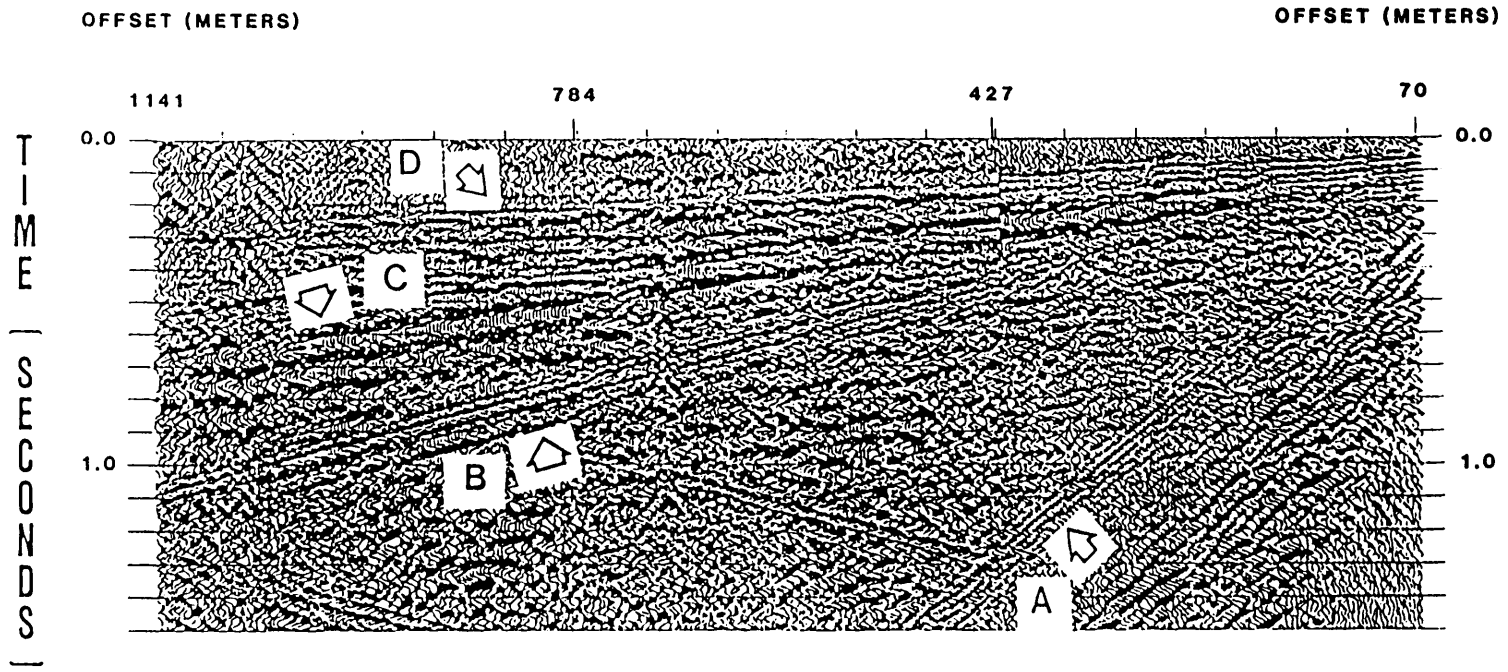

Figure 4. ADCOH Line 1 noise test: (A) Air Wave V_{air} = 0.35 km/s; (B) Direct Wave V_1 = 1.1 km/s; (C) First refracted event V_2 = 2.9 km/s; and (D) Second refracted event V_3 = 6.05 km/s. The direct wave is reflected back from an unidentified interface on shot records 4 and 5 with velocity = 1.1 km/s.

Seismic Data Processing

One of the major objectives of this study is the use of refracted arrivals to image the Brevard fault zone at shallow depths. To make the refracted arrivals useful for interpretation an unconventional data processing flow is introduced in which a concept to produce a refraction stack data is followed. Later, the refraction stack data are combined with the conventional reflection stack data to obtain composite stack sections.

Refracted Arrivals

The standard processing sequence for multifold reflection data requires that refracted wave arrivals be discarded by the application of muting because the NMO correction causes a time variant stretching that effects the early arrivals most. Also, the reflected wavefront follows a hyperbolic time-shift (moveout) between traces with increasing offset while the refracted headwave undergoes a linear increase in time with offset. Refracted arrivals are thereby discarded in favor of reflected events, since both moveout corrections cannot be easily applied to the same data. In this study, the refracted arrivals are evaluated to image near surface structures. The refracted arrivals were reduced to delay times of a common refraction surface.

Where the refraction interfaces are planar, the interpretation of the refraction method follows straight forward processing routines with regular traveltime-distance curves (Palmer, 1986). However, most of the time irregular traveltime-distance curves result from refraction surveys because subsurface geology is represented by non-planar reflectors. Techniques for interpreting irregular traveltime-distance curves are derived from the concept of delay time. For a single seismic interface, the traveltime t of a headwave arriving at a source-receiver distance x is $t = t_0 + \frac{x}{V_2}$ where t_0 is the delay time and V_2 is the refractor velocity (Figure 5a) (Palmer, 1986; and Barry, 1967). Delay time t_0 consists of a source term (t_{CK}) that is the time it takes part of the seismic wavefront to travel to the interface at the critical angle of incidence i_c and a receiver term (t_{Lc}) that is the traveltime for the wave to travel to the receiver from the seismic interface at the angle i_c (Figure 5a). The delay time, therefore, is the traveltime for the critically refracted wavefront to travel from source to refractor then to a receiver located at the critical distance x_c (Figure 5c). Most refracted data are recorded at offset greater than x_c and the traveltime-distance curve will therefore experience a linear increase $\frac{x}{V_2}$ in time with offset called refraction moveout (RMO) (Figure 5b).

To assist in the evaluation of velocities and removal of RMO, the concept of common refraction surface (CRS) ensembles is introduced. CRS gathers are composed of traces of source and receiver pairs symmetric about a common mid-point (CMP) which projects to the mid-point of the CRS (Figure 5a). When CRS ensembles are sorted according to offset, the linear RMO is observed in adjacent traces (Figure 5b and Figure 6a). Common refracted surface ensembles reduced to delay time were used to form the input data for refraction stacks. Removal of refracted moveout would reduce all traces in the CRS ensemble to common delay time. This is displayed in Figure 5d and Figure 6b.

The motivation for the refraction stack is to exhibit refracted arrivals in the form of a vertical seismic section in the profile and delay time domain that is ready for interpretation. Taking advantage of a situation where refracted arrivals are routinely discarded, a scheme was devised to enhance near surface imaging by emphasizing refracted events in seismic data. Processing according

to the concept of a refraction stack enhances the refracted events and displays the stacked data in a fashion similar to reflection seismic sections. A CRS ensemble before RMO correction (a), and after RMO correction (b) is shown in Figure 6. Refracted events showing linear moveout by offset are corrected to represent the same time, t_0 in (b), that is equal to delay time. A stacked trace (c) obtained from stacking the RMO corrected data (b) shows the signal-to-noise ratio enhancement. The refraction stack process shown in Figure 5 and Figure 6 involves five processing stages unique to this method. They are 1) selection of time-offset windows for the first arrivals, 2) sorting data traces into the CRS ensembles, 3) determination of refractor velocity by refraction velocity analysis, 4) application of linear refraction moveout (RMO), and 5) stacking of traces in the CRS ensembles.

This procedure begins by separating the refraction firstbreak wavelet from the rest of the trace creating refraction-only traces that are sorted to give common refracted surface (CRS) gathers. The separation is accomplished by applying a mute function that zeroes the entire trace except for a window that brackets the first arrival wavelet to create refracted data traces. In this study, the window length of 0.1 s is chosen from the autocorrelation function. For consistency, the mute window function is determined and and applied to shot gathers.

The multifold reflection data of CMP may be given by:

$$f_1(t) = f_0(t + \Delta T_1)$$

$$f_2(t) = f_0(t + \Delta T_2)$$

$$\cdot$$

$$f_n(t) = f_0(t + \Delta T_n)$$

where $\Delta T_n = \sqrt{T_0^2 + \frac{x_n^2}{V_1^2}} - T_0$, and $f_0(t)$ represent the normal moveout time and the zero offset trace respectively. T_0 is the two-way zero offset reflection time and V_1 is the reflection velocity. If the traces consist of only reflected events, the CMP stacked trace from the above may be given as:

$$f(t) = \frac{1}{n}\sum_{i=0}^{n} f_i(t - \Delta T_i) \simeq f_o(t)$$

which represents reflected energy at the zero-offset in n-fold data. Similarly, the multifold refraction data may be given as:

$$g_1(t) = g_0(t + \delta t_1)$$

$$g_2(t) = g_0(t + \delta t_2)$$

$$\cdot$$

$$g_n(t) = g_0(t + \delta t_n)$$

where $\delta t_n = t - t_0 = \frac{x}{V_2}$, t_0 is the delay time, and V_2 is the refractor velocity. The CRS stacked trace may be given as:

$$g(t) = \frac{1}{n}\sum_{i=0}^{n} f_i(t - \delta t_i) \simeq g_o(t)$$

which can be considered to represent the refraction event at t_0 delay time for n-fold data. These summation processes can also be used to determine the velocity information needed. In these cases, V_1 is the stacking approximation to the root-mean-square velocity to the reflector, and V_2 is the stacking averaged apparent velocity of the refractor.

Although there is a strong smoothing effect because of refraction stacking, the stacked traces from the CRS ensembles represent two-way traveltimes for critically refracted travel paths (delay time t_0). The difference in two-way traveltime between the refraction delay time t_0 and the two-way time T_0 of zero offset reflected waves is defined by the cosine of the critical angle (Figure 5c). The refraction delay times can be converted to the vertical two-way times by $T_0 = \frac{t_0}{cosi_c}$. This shift is necessary if velocity contrasts or layer thicknesses are such that two-way delay time through the subsurface is visibly different from the corresponding reflected two-way arrival time. As addressed in a later section, the necessary shift for the ADCOH data modelled is less than 4 ms (1 sample interval). Because of this small difference, no shift is applied to the ADCOH Line 1 refraction stack sections.

The smoothing effect on the data by stacking was a major concern. To observe this effect, three CRS groupings with different offset ranges were processed. The CRS offset groups are: (1) All offsets 0.2-4.15 km (RSTACK2); (2) Near offsets 0.2-2.5 km (RSTACK2B); and (3) Far offsets

2.5-4.15 km (RSTACK2A). Refraction stacking velocity analysis is performed separately for each of these offset ranges after respective sorting into these groups.

The CRS gathers are used to determine the correction (refraction) velocity by constant velocity analysis. The velocities are chosen using constant velocity refraction stacks (CVRS). CVRS are generated from panels of adjacent stacked CRS traces that have all been reduced to delay time by RMO correction with the same velocity. The velocity which results in the panel with the best signal to noise ratio (S/N) and refracted continuity is the refraction stacking velocity for that group of adjacent CRS gathers (Figure 7). This refraction stacking velocity is the average refractor velocity from updip and downdip apparent refraction velocities because the data used were from split spread geometries. From CVRS analysis at CRS intervals along the line, the refraction stacking velocities at 25 locations for the entire line are determined. CRS gathers summed into one trace after the most optimum RMO correction applied enhance the refracted signal and attenuated unwanted noise components. Therefore, accurate velocity picking and optimum RMO applications are determined from the evaluation of S/N in CVRS panels.

Stacking of CRS gathers reduced to a common datum of 0.4 km directly followed corrections for refraction moveout. The ADCOH Line 1 data set resulted in three refraction stack sections which all exhibit a very continuous refractor at about 0.1 to 0.2 s with a high S/N. Further improvements in refractor continuity was obtained by application of one pass of surface consistent residual statics. Effect of the application of residual statics improved the data quality with some smoothing effect but the major features are preserved as seen in Figure 8. Three final refraction stack sections are shown in Figure 10.

Reflected Arrivals

The reflected events in the ADCOH regional Line 1 from CMP 710 to 1692 were also reprocessed. The main objective of reprocessing the reflection data was two-fold. First, improvement in shallow (first 0.6 s) data reflection continuity to relate the near surface reflected events with those refracted events in refraction stack sections. Second, enhanced recovery of reflected arrivals especially from the Brevard fault zone to image it from the surface to the depth which it roots into the BRT.

The final reprocessed reflection stacked section was generated following the standard processing sequence for the original data (Çoruh and others, 1987) with the addition of new mute functions, improved velocity coverage, predictive deconvolution, and multi-pass surface consistent residual statics with windowing to enhance the BFZ.

With the application of 35 mute functions, predictive deconvolution, 25 velocity functions, and residual statics, enhanced reflections, from both shallow and deep events, were obtained (Figure 9). The most dramatic iinprovement in reflected data resulted from increased velocity coverage which improved the quality of reflections in the first 0.6 s. Final improvements occurred from multi-pass multi-iteration residual statics with velocity updating. Special windowing for the static shift calculations focused on the subhorizontal reflections at the beginning of the line, then followed the reflections of the BFZ to the surface.

Combined Refraction and Reflection Stacks

As one of the final objectives of this study, specific final refraction and reflection stack sections were combined into composite stack sections for detailed composite interpretation. This was ac-

complished by muting both data sets followed by summing. The mute function of the refraction and reflection stack data were chosen to taper out the refracted events while beginning to taper in the reflection events in the stacking to generate the composite stack (Figure 13). When matching CMP trace pairs from both refracted and reflection stack sections were not present, a zero trace was added in place of the missing CMP trace. This procedure is responsible for the gap at the top of CMP 1145 to CMP 1160 through the absence of refracted stack traces and the gaps at CMP 1410 and 1590 due to the absence of reflection stack traces.

The composite stack section is migrated further increasing S/N and refraction and reflection continuity. As a result of these improvements, the migrated composite stack section (Figure 14) will be used in the final interpretation. The data gap between CMP 790 and 870 in the reflection data, as a result of acquisition through the town of Westminster, South Carolina, has created edge effects from migration.

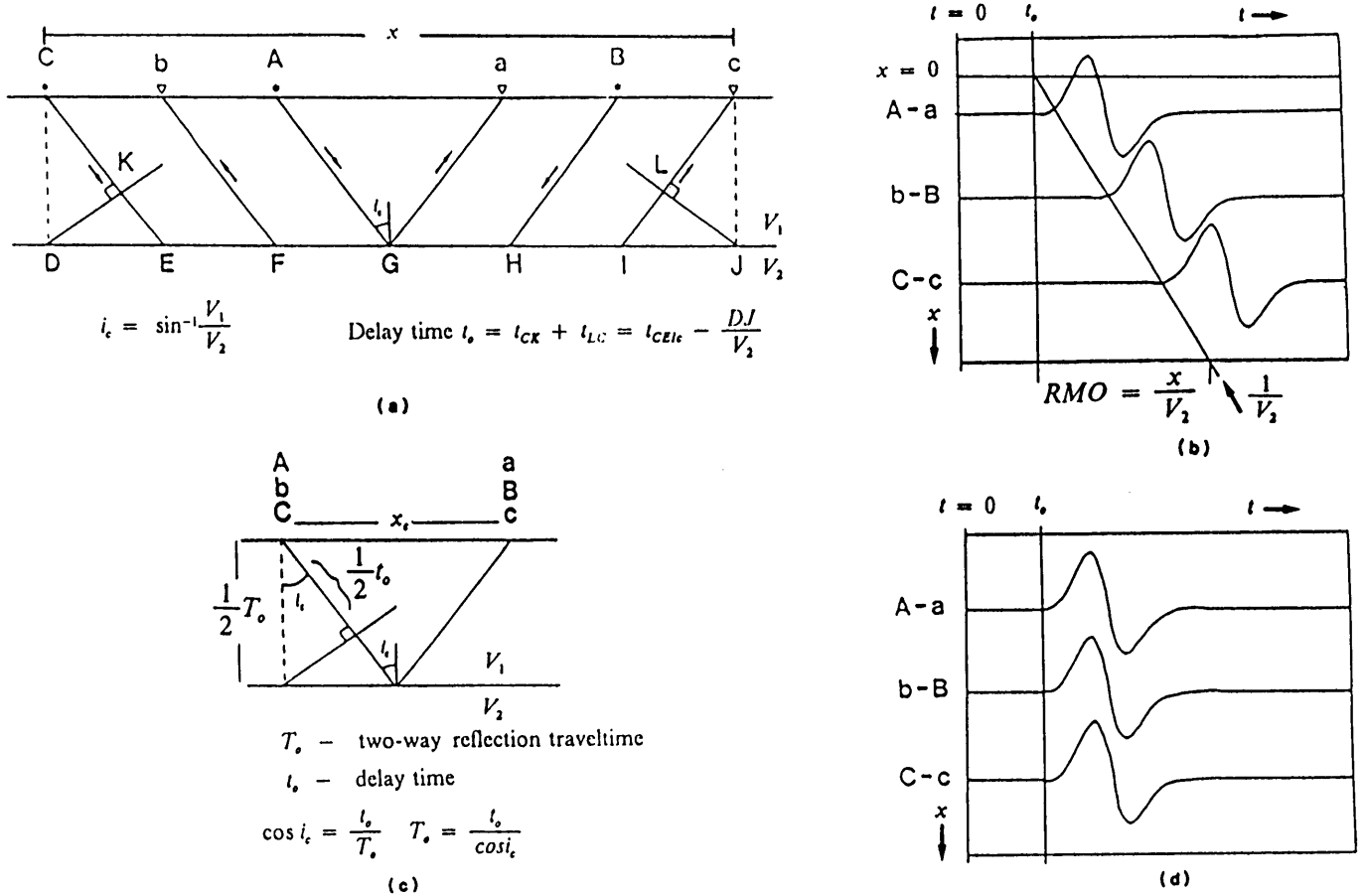

Figure 5. **Concept of the refraction stack processing:** In these figures A,B,C and a,b,c letter sets indicate the locations of source and receiver, respectively. (a) Diagram of CRS ensemble from split spread data set along a two-layer model. Travel time for the refracted wave associated with, for example, the path CEIc is composed of a delay time (t_o) term and a RMO (x/V_2) term. (b) The resulting traces in the CRS gather display a time-offset relationship for the linear refraction moveout increase in time with offset. (c) Diagram of the CRS gather after RMO correction, all travel paths are reduced to delay time which can be represented by the critically reflected travel path. (d) Corresponding traces in the CRS gather following RMO removal. All traces are observed with the first arrivals at time t_o regardless of offset.

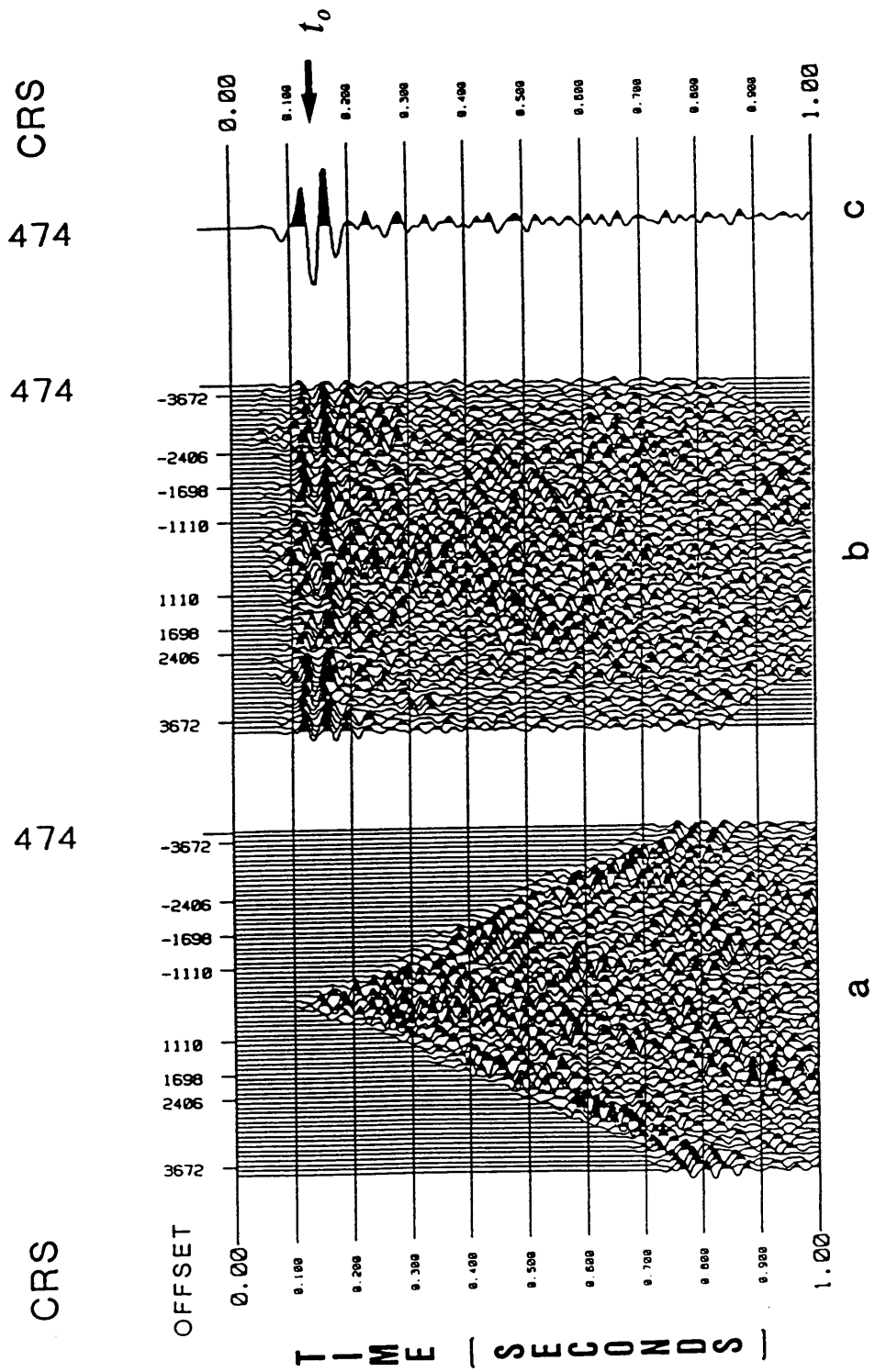

Figure 6. **Refraction stack processing:** (a) CRS ensemble from the 0.2-4.15 km offset range. Mute is only applied before the first arrival, in this case, to demonstrate ability of refraction stack to enhance refracted events. (b) CRS gather following RMO correction. First arrivals are reduced to delay time t_o. (c) Stacked trace from CRS gather. Note that the delay time t_o is equal to the vertical , one-way reflection time multiplied by the cosine of the critical angle i_c.

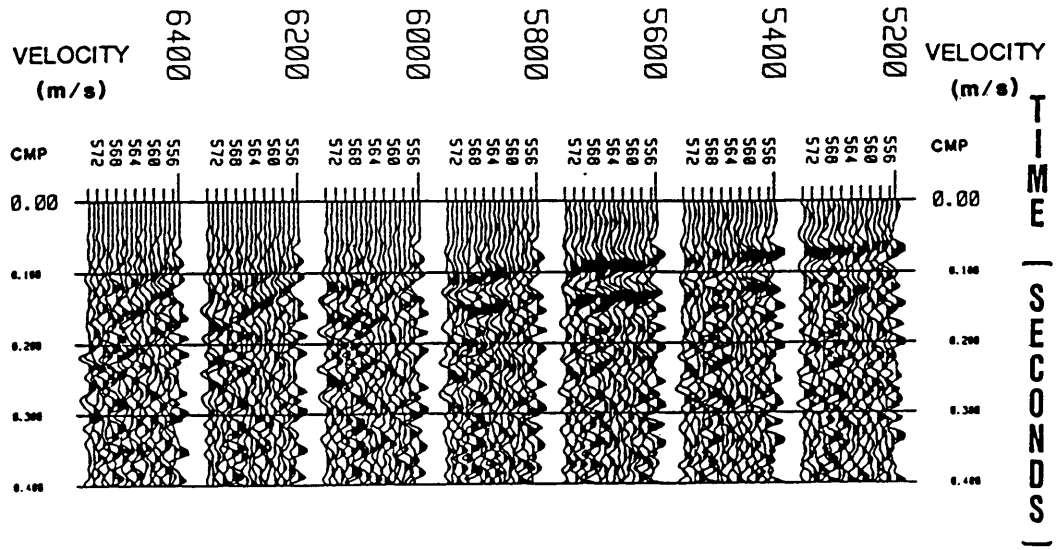

Figure 7. Constant velocity refraction stack (CVRS) panels: Refraction moveout velocity (5.6 km/s) is chosen from this panel with the highest signal-to-noise ratio.

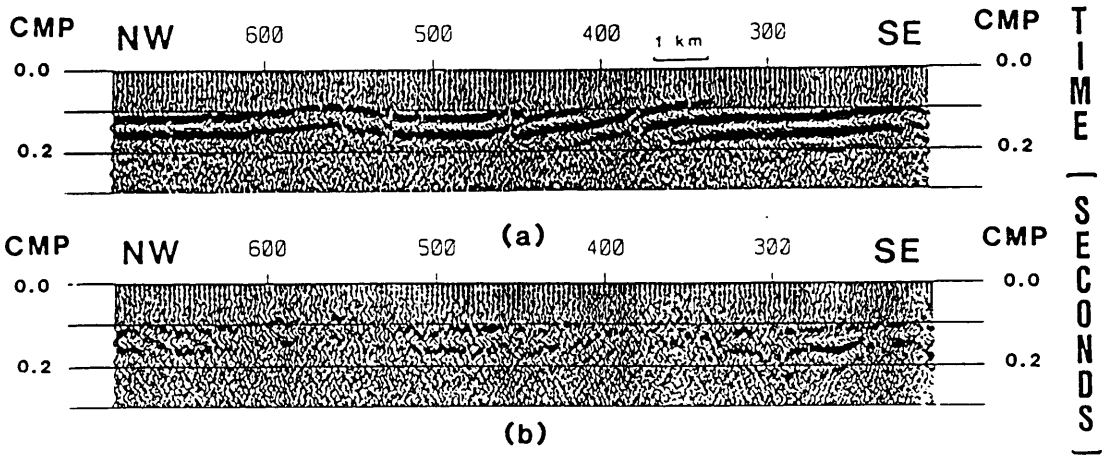

Figure 8. Residual statics improvements in refraction stack sections: RSTACK2 after (a) and before (b) application of surface consistent residual statics.

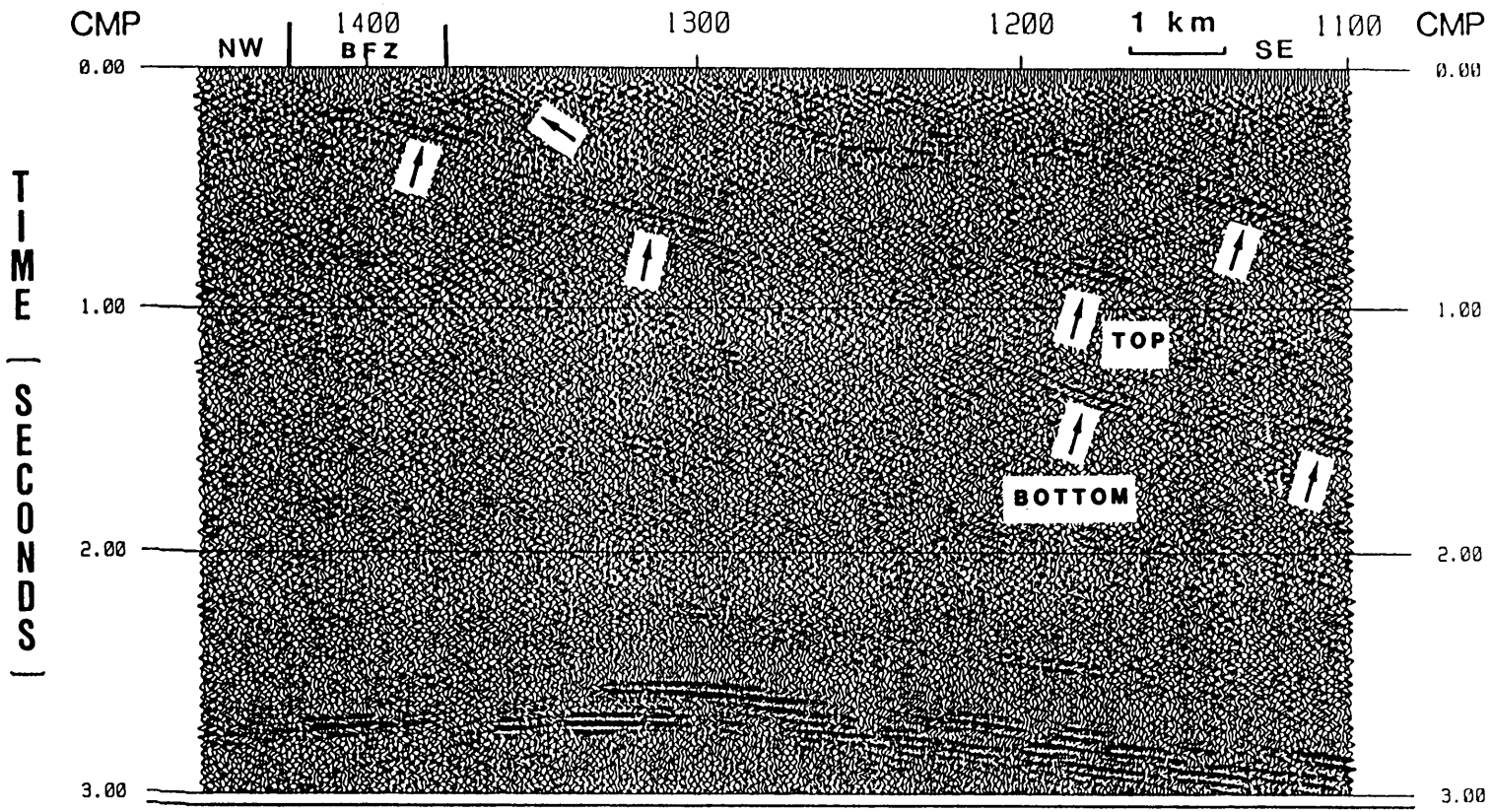

Figure 9. **Portion of reprocessed ADCOH regional** Line 1 reflection stack section: Improvements in shallow and BFZ reflections, indicated by arrows, result from 35 new mute functions, predictive deconvolution, increased velocity coverage at 25 CMP gathers, and one pass of surface consistent residual statics. The arrows labelled TOP and BOTTOM locate the upper and lower boundaries of the BFZ.

Discussion and Interpretation

In order to extend the interpretation of ADCOH regional Line 1 seismic data, two points must be addressed: 1) the subsurface imaging capabilities of the refraction stack method and its limitations, and 2) determination of the nature of the well defined refractor, in the refraction stacks, in terms of geologic interfaces. The noise test is examined to identify the refracted events in the refraction stack. Lithologies from ADCOH DH1 shallow core hole were used for correlation of the refraction data with near surface geology.

Ability of Refraction Stacks to Image the Subsurface

The refraction stack sections after the application of residual statics are shown in Figure 10a, b, and c for the offset ranges 0.2-4.15 km, 0.2-2.5 km, and 2.5-4.15 km, respectively. These figures clearly show that refraction stacks as seismic sections have a high S/N ratio. The smoothing effect of multi-offset data on the resolution of the data is the most important feature to be addressed. Since the surface covered by the refracted wave in the CRS ensemble is sampled more by the large offset range data, the smoothing is directly proportional to offset ranges. Because of larger refracted ray paths, large offset traces are also approximated the most by assuming subhorizontal refractors.

As with reflection data, smoothing will also result from the summation process of multifold data compostion. To observe these results of offset and fold upon refraction resolution, three different trace offset ranges were applied to generate refraction sections. The near and far offset range sections should exhibit more detail than the total offset range section due to lower fold. When the multiplicity of the data is equal, the near offset section has more resolution than the far offset section because each CMP with near offsets sums traces with shorter sampling paths. The complete offset range stack will display the least detail of the three stack sections. On the other hand, this section will have the best S/N and refractor continuity which is desirable in areas of low seismic reflectivity.

Comparison of all three refraction stack sections (Figure 10) show that RSTACK2 (Figure 10a) has the best refractor continuity. As expected, all three sections display different detailed features while broad features are similar for all three. The sections exhibit breaks in refractors with vertical offsets. Particularly noticeable examples common in all three sections are the distinct breaks in the refraction events near CMP 450 and 730 (F1 and F2 in Figure 10). As a cross check, shot gathers are examined in detail using a standard refraction prospecting technique to confirm that the fault signatures are contained in the reversed refraction time-distance curves. To accomplish this, shot record 260 at CMP 706 and shot record 290 at CMP 766, one from each side of the apparent fault, are given with respective time-distance curves. These reversed time-distance curves covering CMP 730 are given in Figure 11. Clearly observed from Figure 11 is a negative time shift of 0.029 s in the shot gather (260) with source at CMP 706 and a positive time shift of 0.033 s in the shot gather (290) with source at CMP 766. The negative time shift occurs in all traces recorded, from shot 260, to the northwest of CMP 750. The positive time shift occurs in all traces, from shot 290, to the southeast of CMP 721. Modelling from this t-x curve, with V_1 = 1.67 km/s and V_2 = 6 km/s (i_c = 18°), the fault is located beneath CMP 734 with the downthrown side to the southeast (Figure 11). Taking the time shift dt = 0.031 s, the offset on this fault (dz) is about 52 m. In Figure 10a the fault is located at CMP 730 with the offset (dt) of 0.03 s on the downthrown side to the southeast. This same procedure yields similar results when applied at CMP 450 locating

the fault at CMP 447 with an offset of 0.025 s. In most cases, detailed features such as refractor undulation and discontinuities are displayed on both RSTACK2A (Figure 10c) and RSTACK2B (Figure 10b) while not usually observed on RSTACK2 (Figure 10a) because of a high degree of smoothing. Judging from all sections, the full offset range refraction stack (Figure 10a) exhibit the common features because uncommon features are smoothed out. Note the refractor displacement (F3) at CMP 920 in Figure 10b and Figure 10c which is not visible in Figure 10a while the displacements at CMP 350, 450, and 730 are common in all stacks. This is believed to be due to the higher smoothing in RSTACK2 than in RSTACK2A or RSTACK2B. With respect to these general features, the different seismic signatures are observed on all three sections for each major geologic province. With respect to smoothing, the near and far offset range stack sections display more apparent refractor detail. The far offset section (Figure 10c) appears to display more refractor undulation than the near offset section (Figure 10b). After close examination though, the trace-to-trace detail is discovered to be small with refractor variations emphasized by lower fold. Differences between RSTACK2A (Figure 10c) and the other two refraction stack sections (Figure 10a and 10b) are also possibly due to the depth which the far offset travel paths reach. Since folding is a major cause of smoothing, the far offset travel paths in RSTACK2 (Figure 10a) are averaged out by the same number of short travel paths.

Correlation of available data sets

For a correlation of arrivals from refraction stack sections with lithology and geologic structure, the ADCOH regional Line 1 noise test, conducted at the beginning of the line, is examined with the purpose of obtaining a model for the shallow geology in the Inner Piedmont allochthon which is developed from refracted arrivals. Since the noise test was recorded with 3 m (10 ft) trace intervals that resulted in a 5.4 km far offset survey, all major refractors that are present in the ADCOH regional Line 1 data were examined.

The analysis of the noise test reveals that two principle refracted events are recorded in addition to the direct wave (Figure 12). The velocities of these three arrivals as determined from the shot records are: $V_1 \simeq 1.1$ km/s for the direct wave; $V_2 \simeq 2.9$ km/s for the first refractor; and $V_3 \simeq 6.05$ km/s for the second refractor. The two refracted waves and the direct wave imply a three-layer subsurface model with two distinct seismic interfaces. Since the wave velocity in each layer has already been determined, all that is necessary to determine the thickness of the first two layers is the zero-offset delay times for the two refraction events. Taking the intersection of the air wave and the direct wave as the zero-offset source point, the two-way delay times for the two refracted events as picked from the shot records are: (1) $t_1 \simeq 0.05$ seconds for Refraction A. and (2) $t_2 \simeq 0.065$ seconds for Refraction B (Figure 12). Using the traveltime equations, the thicknesses of the first layer (h_1) and the second layer (h_2) are calculated to be 30 m and 37 m respectively. Of additional interest in this study are the two crossover distances (x_{C1}, x_{C2}) . Substituting the delay-times and seismic velocities observed from the noise test for the first two layers into the appropriate traveltime equations and solving for offset leaves the distance at which the first refraction arrives before the direct wave x_{C1} at 89 m. Similarly, the second refraction becomes the first arrival x_{C2} at 142 m and remains the first arrival throughout the 5.4 km of offset for the noise test. These distances are also observed in the actual time-distance curves given in Figure 12.

This result supports our main RMO stage assumption that all traces in a CMP gather from 0.2 to 4.15 km offset can be moved-out at the same apparent refractor velocity. Using the parameters obtained from the noise test, a difference of less than 0.004 s is found between refraction delay time and two-way vertical reflection time. Since the sample interval is 0.004 s, the correction for this difference was not applied.

The bright refraction event in the refraction stack is evaluated to be representative of the second refractor, interpreted from the noise test at a depth of 67 m with an intercept time of 0.065 s. The time, measured between the surface elevation mark and the refractor, in the refraction stack is also 0.065 s at the same location (CMP 205) as the noise test. The refractor is interpreted to continue

from the location of the noise test (CMP 202) to CMP 980 (Figure 10) at which it occurs at a two-way delay time of 0.025 s from the surface elevation mark to the refractor. Located near CMP 980 on Line 1, there is shallow ADCOH hole DH1 to a depth of 0.3 km. As calculated from the three-layer model, average velocity to the second refractor is $\simeq$1.67 km/s. Assuming that this average velocity is relatively constant between CMP 980 and the beginning of the line, 0.025 s two-way delay time converts to 0.026 s two-way traveltime. This corresponds to a depth of 21 m. This depth correlates within 7 m to the boundary logged in DH1 between the weathered zone and a granitic gneiss.

Interpretations

The extended interpretation of the ADCOH regional Line 1 seismic data, composite stack using automatic line drawing, parallels those of Çoruh and others (1987) and Hatcher and others (1987b) with an expansion on the BFZ and the addition of shallow refraction information. In addition to the seismic data, previous surface geological studies are incorporated to constrain interpretations of near surface events.

Results of the noise test and shallow core hole data analysis lead to an interpretation of the refractors as the bottom of the double layer weathered zone (surface of bedrock) with an average velocity of 1.67 km/s. Additionally, this interpretation is supported by surface geology where some correlation is found between lithologic units and refractor quality. The refractor is best seen where amphibolite, granitic gneiss, and Henderson gneiss are exposed at the surface. The refractor is poor below Poor mountain amphibolite possibly because of geometrical complexity of the seismic interfaces. The Brevard fault zone and Rosman fault to the west are indicated by a no-data window between CMP 1390 and 1430 to 0.1 s depth. In the eastern Blue Ridge rocks, good refractor segments tend to correlate with greywacke-schist-amphibolite on the surface (Hopson and Hatcher, personal communication). Apparent in the composite stack section is the signature of the three

major tectonic provinces. The Inner Piedmont allochthon and Chauga Belt (IPA-CB) possess a relatively simple continuous surface below the weathered layer (Figure 14). Near the boundary of the IPA-CB a decrease in refraction continuity is observed. A strong reflected event can be projected upward to this approximate location at the surface and is interpreted as the CB-IPA boundary (CB/IPA) at depth. In other parts of the composite section, reflectors are traced near such tectonic boundaries at the surface and could be evidence of major lithologic boundaries. The decrease in refraction continuity near the CB/IPA is slight in comparison with the one exhibited at the BFZ to Chauga Belt interface. The surface signature of the Brevard fault zone can best be described by a lack of refracted seismic signal up to 0.1 s (Figure 14). The refracted signal begins to reappear in the Blue Ridge allochthon as a refractor with relatively high S/N but with many discontinuities (Figure 14) that possibly indicates inhomogeneity. The refracted events in the BRA are completely different from those in the IPA/CB as well as the major tectonic boundary (BFZ) that divides them. Although both have a relatively high S/N ratio, the refracted events are discontinuous at higher angles with truncations occurring.

An automatic line drawing (ALD) of the unmigrated composite stack section (Figure 15) was generated for additional detailed interpretation. In this form, an increase in reflection coherency over the composite stack was obtained. One of the most improved targets of this study is the BFZ. From the surface, where the BFZ is distinguished in the refractions, to 6 km depth (2 s) the Brevard fault zone can be seen in more detail than previously published. As originally stated by Clark and others (1978), the upper and lower boundaries of the BFZ are imaged as relatively continuous eastward-dipping reflectors. Figure 15 shows that the Brevard fault has a larger zone than is mapped on the surface. When the boundaries from surface mapping are considered the upper and lower boundaries are close together near the surface (0.2 s), move apart to a maximum distance of 0.7 s near 1 s depth (3 km) below CMP 1200, then splay together into the BRT at 2.0 s (6 km) (Figure 15). But the composite stack section in Figure 15 shows that the Brevard fault zone has a relatively constant thickness, which dips 17°, to a depth of 4.2 km where it flattens to a dip of 8°. Between the top and bottom boundaries, the interior of the BFZ is imaged as reflective zones

with east dipping packages of reflectors. The Brevard fault zone image is more complex than described in previous literature. Instead of thinning at the BRT as its root, the BFZ splays from the Blue Ridge thrust with some considerable thickness (0.6 km). An alternative interpretation (Figure 15) for the Blue Ridge thrust (BRT) places it at a minimum depth of 0.5 s (1.5 km) right below the BRA after paralleling the BFZ as it shallows from 2 s to 1 s depth although a deeper thrust (DT) is also clearly visible at depths of 1 s (3 km) and 2.8 s (8.4 km). In the other direction, the BRT splits as it joins with the BFZ at approximately 2 s (3 km) depth and joins with the deeper trust isolating two distinct tectonic packages between the BRT and DT. The ALD profile displays two other major reflection packages. These are reflector packages which are imaged dipping eastward (Figure 15). From published line drawings (Çoruh and others, 1987) these reflectors eventually become westward dipping to the southeast and are therefore interpreted as major lithologic boundaries in the Six Mile Synclinorium.

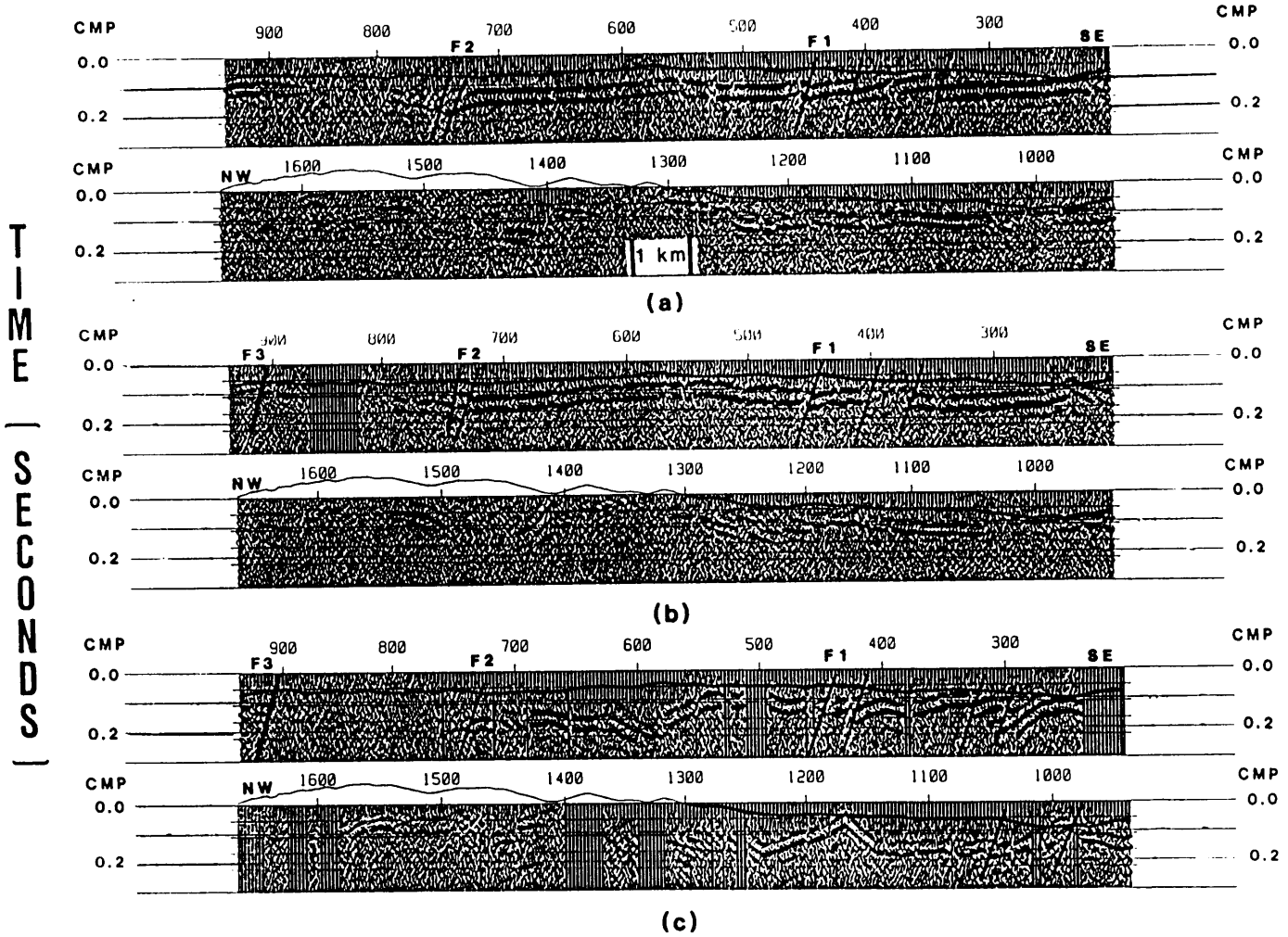

Figure 10. Refraction stack sections with surface elevation plots: (a) 0.2-4.15 kilometer offsets in CRS gathers (RSTACK2). (b) 0.2-2.5 kilometer offsets in CRS gathers (RSTACK2B). (c) 2.5-4.15 kilometer offsets in CRS gathers (RSTACK2A). These sections have had one pass of surface consistent residual statics applied.

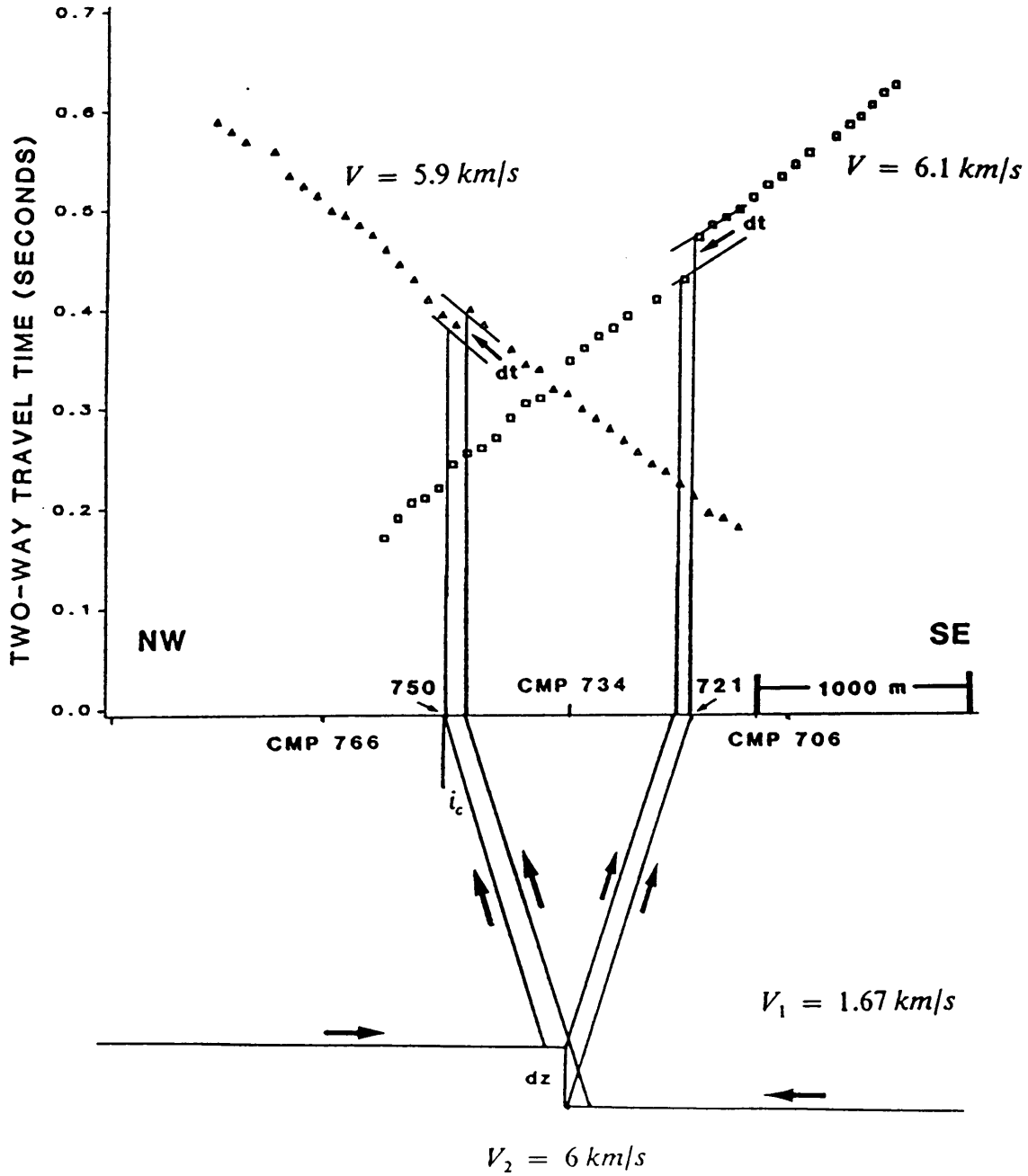

Figure 11. **Fault signature in shot gathers:** Firstbreak arrival times from shot records (260 and 290) that are aligned so that traces from common receiver overlap. The subsurface structure model from the observed first arrival patterns is included using i_c = 18°. The fault is located beneath CMP 734 with an offset of 52 m.

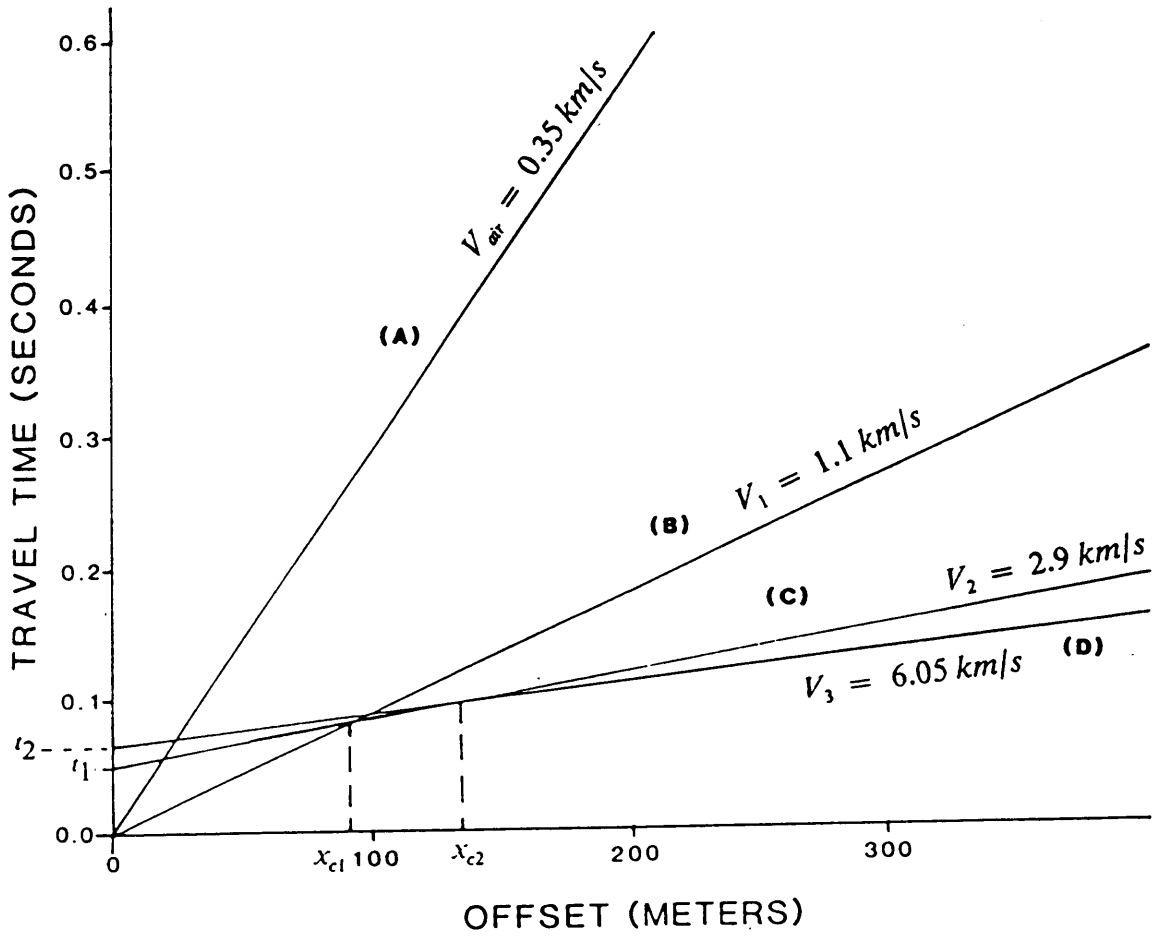

Figure 12. Travel time-offset (t-x) curve of noise test.: Travel time curve for (A) Air wave (V_{air} = 0.35 km/s), (B) Direct wave (V_1 = 1.1 km/s), (C) First refracted wave (V_2 = 2.9 km/s), and (D) Second refracted wave (V_3 = 6.05 km/s), with intercept times (t_1 = 0.05 *s*, t_2 = 0.065 *s*) and crossover distances (x_{c1} = 89 *m*, x_{c2} = 142 *m*).

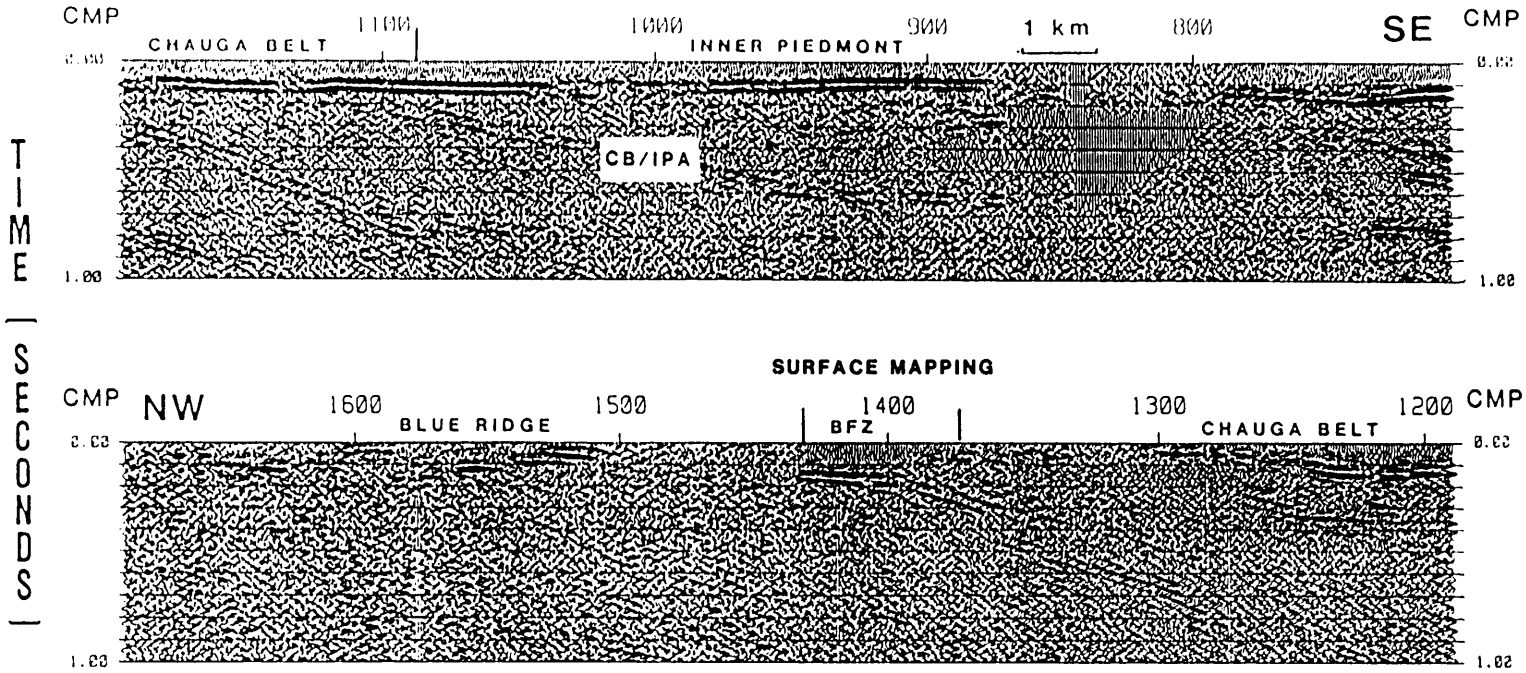

Figure 13. Portion of the composite stack section: 1 second of composite stack section for correlation of refracted and reflected events.

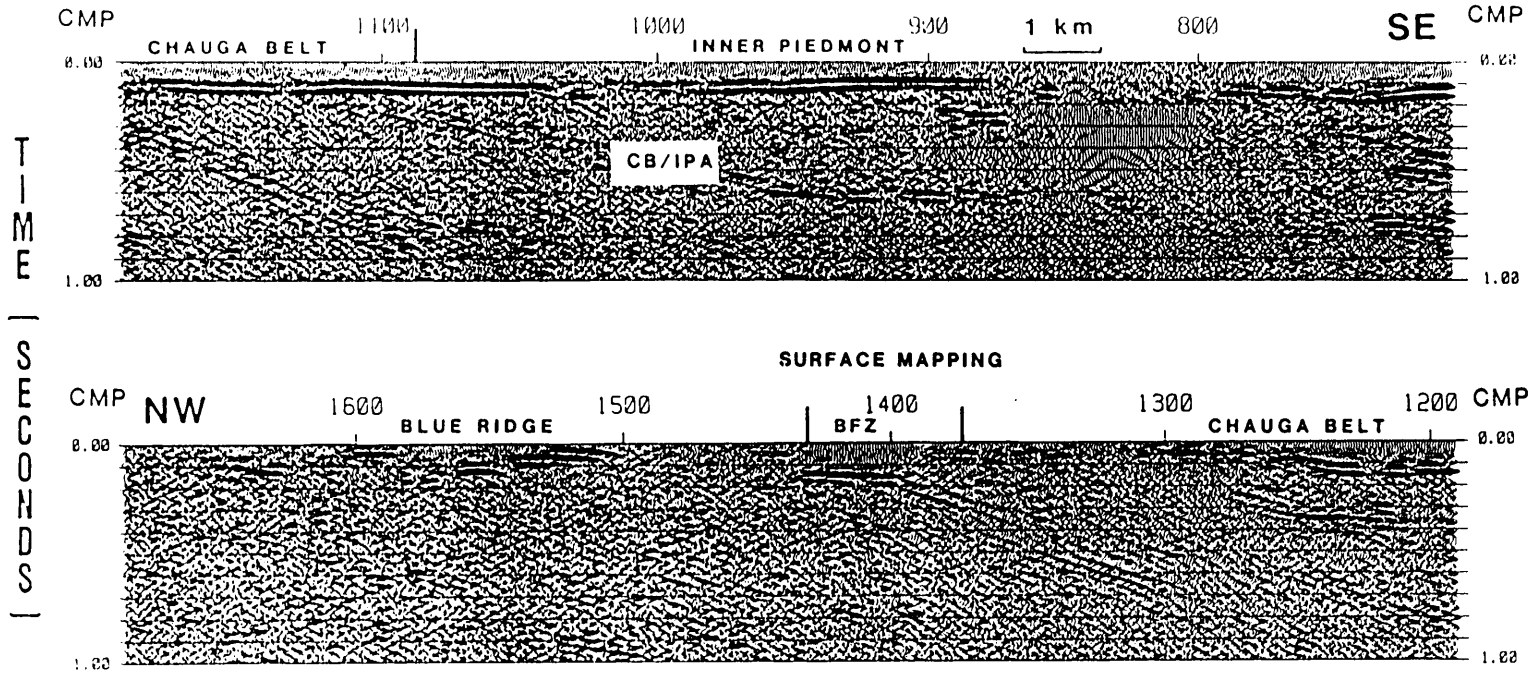

Figure 14. Portion of the composite stack section after migration: 1 second of composite stack section for correlation of refracted and reflected events.

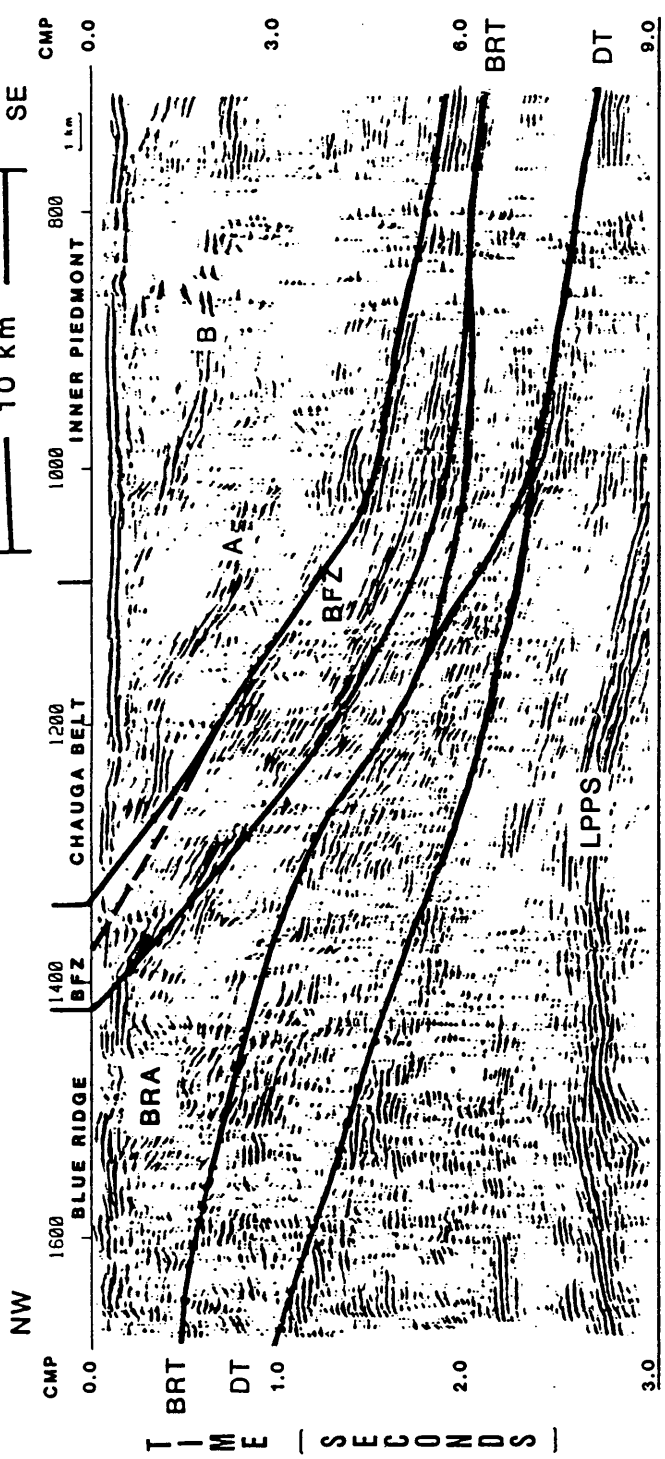

Figure 15. Final automatic line drawing from composite stack section: The BFZ is imaged as a distinct package, with reflections recovered from both the top and bottom as well as from within. Apparent dip of the BFZ is 17° between the surface and a depth of 4.2 km. Between the depths of 4.2 km and 6 km it shows an apparent dip of 8°. These apparent dips correspond to 18° and 9° of true dips, respectively. The BFZ maximum thickness is 0.6 s (1.8 km) and thins as it splays into the BRT. Blue Ridge thrust (BRT) splits to join with the deeper trust (DT) separating two distinct tectonic units. Lower Paleozoic platform strata (LPPS), relatively undeformed, are well imaged below these tectonic packages. Reflective zones (A) and (B) within the Inner Piedmont and Chauga Belt are interpreted to be lithologic boundaries with strong acoustic impedance contrasts. This data shows a larger zone for the Brevard fault than the zone (BFZ) mapped on the surface.

Conclusions

Imaging of the ADCOH Line 1 data set was enhanced through the introduction of composite stack processing. Refracted first arrivals from seismic reflection data were processed using the refraction stack method to generate refraction delay time seismic sections for shallow information. Despite large offsets and high fold, resolution of refracted events is high enough to aid in the interpretation of composite stack sections. These refractors in the refraction stack sections are interpreted to be the lower boundary of the low-velocity weathered layer in the Inner Piedmont and Chauga Belt as well as parts of the Brevard fault zone and Blue Ridge. The average velocity to the refractor is 1.67 km/s in contrast with stacking velocities for the reflection stack data that range from 4.6 km/s to 6.6 km/s. A velocity of 6 km/s was applied for depth calculations for reflected events.

Distinct seismic refraction signatures are associated with the three major geologic provinces in the study area. The Inner Piedmont is recognized as continuous refractions with a high S/N that give way to the Chauga Belt's more discontinuous nature. The shallow Brevard fault zone is distinctive because of its lack of strong coherent imaging by the refraction stack method. Strongly segmented, high S/N refractors possibly indicating inhomogeneity are typical of the Blue Ridge. Reprocessing of the reflected data not only increased the reflectivity of the shallow (first 0.6 s) information but provided improvements in imaging from the Brevard fault zone and shallow

lithologic boundaries in the Inner Piedmont as well as the Blue Ridge. An increase in velocity coverage, in offset and time, as well as residual statics improvements through windowing are responsible for most of these improvements in the deeper events while improved mute functions and predictive deconvolution recovered the shallow reflectivity. The Chauga Belt and Inner Piedmont exhibit both distinct reflection and refraction boundaries. While the Chauga Belt Inner Piedmont interface is displayed as a decrease in refractor continuity, a strong reflection event can be traced to the surface at this same location. The Brevard fault zone and Blue Ridge thrust are seen in greater detail than previously published leading to alternative interpretations of both the BFZ and the BRT. For the BFZ, the highly reflective top and bottom boundaries are well imaged along with reflections from the interior. Reflections from within are recovered as east-dipping packages of reflectors. The Brevard fault zone is about 1 km wide in outcrop as mapped on the surface, reaches a maximum vertical thickness of 2 km at 3 km depth, then thins as it joins into the Blue Ridge thrust at 6 km depth. From the surface to 4.2 km the BFZ dips 17°, between 4.2 km and 6 km the BFZ flattens to an 8° dip. From this point, the Blue Ridge thrust shallows with the BFZ toward the northwest end of the line to a depth of 1.5 km. To the southeast, a short thrust segment connects the BRT with a deeper thrust (DT) located between the BRT and and the undeformed lower Paleozoic platform strata (LPPS). The DT is clearly seen to shallow from approximately 8.4 km depth to 3 km at the northwest end of the line. The BRT and DT isolate two wedge packages observed below the BFZ and above the LPPS.

Bibliography

Barry, K.M., 1967, Delay time and its application to refraction profile interpretation, in Seismic Refraction Prospecting, ed., Musgrave, A.W., Tulsa, Soc. Explor. Geophys., pp. 348-361.

Behrendt, J.C., 1986, Structural interpretation of multichannel seismic reflection profiles crossing the southeastern United States and the adjacent continental margin--decollements, faults, Triassic(?) basins and Moho reflections, in Reflection Seismology: The Continental Crust, eds., Barazangi, M. and Brown, L., AGU Geodynamics Series, v. 14, pp. 201-213.

Brown, L.D., Barazangi, M., Kaufman, S., and Oliver, J., 1986, The first decade of COCORP: 1974-1984, in Reflection Seismology: A Global Perspective, eds., Barazangi, M. and Brown, L., AGU Geodynamics Series, v. 13, pp. 107-120.

Bryant, B., and Reed, J.C., Jr., 1970, Structural and metamorphic history of the southern Blue Ridge, in Fisher, G.W., Pettijohn, F.J., Reed, J.C., Jr., and Weaver, K.N., eds., Studies of Appalachian geology: central and southern, New York, Wiley-Interscience, pp. 213-225.

Chowdhury, K.R., and R.A. Phinney, 1987, Improved resolution of reflections from the crystalline upper crust, Geophys. J. R. astr. Soc., v. 89, pp. 35-40.

Clark, H.B., Costain, J.K., and L. Glover, III, 1978, Structural and seismic reflection studies of the Brevard ductile deformation zone near Rosman, North Carolina, Amer. Journ. of Scie., v. 278, pp. 419-441.

Cook, F.A., Albaugh, D.S., Brown, L.D., Kaufman, S., Oliver, J.E., and Hatcher, R.D., 1979, Thin-skinned tectonics in the crystalline southern Appalachians: COCORP seismic reflection profiling of the Blue Ridge and Piedmont, Geology, v. 7, pp. 563-567.

Çoruh, C., Costain, J.K., Hatcher, R.D., Jr., Pratt, T.L., Williams, R.T., and Phinney, R.A., 1987, Results from regional vibroseis profiling: Appalachian Ultra-Deep Core Hole site study, Geophys. J. R. astr. Soc., v. 89, pp. 147-156.

Costain, J.K., Çoruh, Cahit and Hatcher, R.D., Jr., 1987, Geophysical signature of an inclined strike-slip duplex in the southeastern United States, Geological Society of America, Abstracts with Programs, v. 19, n. 7, p. 628.

Costain, J.K., Çoruh, C., Pratt, T.L., Hatcher, R.D., Glover, L., III, Phinney, R.A., Diebold, J., Williams, R.T., and Zoback, M., 1986, Seismic signatures of tectonic lithofacies from regional lines, Appalachian Ultradeep Core Hole (ADCOH) site area, Fifty-Six Annual International Meeting of Society of Exploration Geophysics, Expanded Abstracts, pp. 136-139.

Hadley, J.B., and Nelson, A.E., 1971, Geologic map of the Knoxville quadrangle, North Carolina, Tennessee, and South Carolina, U.S. Geol. Survey Misc. Geol Inv. Map I-645, scale 1/250,000.

Hatcher, R.D., Jr., Williams, R.T., Costain, J.K., Çoruh, C., Phinney, R.A., Chowdhury, K.R., and Decker, E.R., The Appalachian Ultradeep Core Hole (ADCOH) Project, (in press).

Hatcher, R.D., Jr., Williams, R.T., Costain, J.K. and Çoruh, Cahit, 1987a, Palinspastic reconstruction of the southern Appalachians, Geological Society of America, Abstracts with Programs, v. 19, n. 7, p. 696.

Hatcher, R.D., Jr., Costain, J.K., Çoruh, C., Phinney, R.A., Williams, R.T., 1987b, Tectonic implications of new Appalachian Ultra-Deep Core Hole (ADCOH) seismic reflection data from the crystalline southern Appalachians, Geophys. J. R. astr. Soc., v. 89, pp. 157-162.

Hatcher, R.D., Jr., 1971, Stratigraphic, petrologic, and structural evidence favoring a thrust solution to the Brevard problem, Amer. Jour. Scie., v. 270, pp. 177-202.

Jonas, A.I., 1932, Structure of the metamorphic belt of the southern Appalachians, Amer. Journ, Scie., v. 224, pp. 228-243.

King, P.B., 1955, A geologic section across the Southern Appalachians-an outline of the geology in the segment in Tennessee, North Carolina and South Carolina, in Russell, R.J., ed., Guides to southeastern geology, Boulder, Col., Geol. Soc. America Guidebook, pp. 332-372.

Palmer, D., 1986, Refraction Seismics the lateral resolution of structure and seismic velocity, eds., Helbig, K. and Treitel, S., London, Geophysical Press, 269 p.

Reed, J.C., Jr., and Bryant, B., 1964, Evidence for strike-slip faulting along the Brevard zone in North Carolina, Geol. Soc. America Bull., v. 75, pp. 1177-1196.

Appendix

FIGURE	PROGRAM	DATASET	PROJECT	TAPE
Figure 4	FIG04.DAT	NVSW1	DEEP1	B0037
Figure 6	FIG06.DAT	MUTESRT2	DEAP1	B0037
Figure 7	FIG07.DAT	MUTESRT2	DEAP1	B0037
Figure 8	FIG08.DAT	RSTACK2	DEAP1	B0037
Figure 9	FIG09.DAT	FINAL1	DEEPBFZ	B0037
Figure 10a	FIG10.DAT	RSTACK2	DEAP1	B0037
Figure 10b	FIG10.DAT	RSTACK2B	DEAP1	B0037
Figure 10c	FIG10.DAT	RSTACK2A	DEAP1	B0037
Figure 13	FIG13.DAT	COMP2	DEEPBFZ	B0037
Figure 14	FIG14.DAT	MIG_COMP2	DEEPBFZ	B0037
Figure 15	FIG15.DAT	COMP_LD1	DEEPBFZ	B0037

Table 1. Figures-located on backup B0037-KJL.BCK

The vita has been removed from the scanned document